nature portfolio

https://doi.org/10.1038/s41567-021-01310-3

Supplementary information

Emergence of spin singlets with inhomogeneous gaps in the kagome lattice Heisenberg antiferromagnets Zn-barlowite and herbertsmithite

In the format provided by the authors and unedited

Supplementary information for "Emergence of spin singlets with inhomogeneous gaps in the kagome lattice Heisenberg antiferromagnets Zn-barlowite and herbertsmithite"

Jiaming Wang[1], Weishi Yuan[1], Philip M. Singer[2], Rebecca W. Smaha[3,4],
Wei He[3,5], Jiajia Wen[3], Young S. Lee[3,6], and Takashi Imai[1,7]*
[1]*Department of Physics and Astronomy, McMaster University, Hamilton, Ontario, L8S 4M1, Canada*
[2]*Department of Chemical and Biomolecular Engineering, Rice University, 6100 Main St., Houston, TX 77005, USA*
[3]*Stanford Institute for Materials and Energy Sciences, SLAC National Accelerator Laboratory, Menlo Park, CA 94025, USA*
[4]*Department of Chemistry, Stanford University, Stanford, CA 94305, USA*
[5]*Department of Materials Science and Engineering, Stanford University,Stanford, CA 94305, USA*
[6]*Department of Applied Physics, Stanford University, Stanford, CA 94305, USA and*
[7]*Brockhouse Institute for Materials Research, McMaster University, Hamilton, Ontario, L8S 4M1, Canada*

I. $1/T_1$ RESULTS

In Fig. S1(a), we present additional examples of the stretched exponential fit of the recovery curve $M(t)$ observed for the ^{63}Cu sites in $ZnCu_3(OD)_6FBr$. The fit appears reasonable down to $\sim$30 K, where $1/T_{1,\rm str}^{\rm Cu} \simeq 10^3$ s^{-1}. Notice that even at $\sim$20 K and below, $M(t)$ initially recovers as fast as at 30 K in the short time regime up to $t \sim 0.5$ ms, followed by slower recovery in the long time regime. The contribution of the slow mode gradually increases with decreasing temperature, and $M(t)$ clearly exhibits a kink at $t \sim 1$ ms around 4.2 K. These findings imply that a substantial fraction of ^{63}Cu sites still relax with the same fast relaxation rate $1/T_1^{\rm Cu} \simeq 10^3$ s^{-1} even at 4.2 K, but an increasing fraction of ^{63}Cu sites have much slower relaxation rate at lower temperatures. The stretched fit cannot reproduce this crossover behavior from the fast to slow relaxing component, and the fit becomes increasingly poor below 30 K. This is because the stretched fit implicitly assumes that the distribution is single-peaked. We also note that apparently good stretched fit with the stretched exponent β close to 1 does not necessarily guarantee that the distribution of $1/T_1$ is single-peaked and centered around one value of $1/T_1$. As we demonstrated earlier with a counter example in Fig. 1 of [1], one might accidentally find that the stretched fit appears reasonably good even if $1/T_1$ has two distinct components.

In Fig. S1(b), we present the results of the inverse Laplace transform (ILT) fit of $M(t)$. The fits are good even below 30 K. A major thrust of the ILTT$_1$ analysis is that we do not assume any particular form up front for the density distribution function $P(1/T_1)$. If $1/T_1$ has only one component with very little distribution, one will find a narrow, single-peaked $P(1/T_1)$; the resulting ILT fit of $M(t)$ becomes similar to a single-exponential fit. On the other hand, if there are two distinct values in the distribution of $1/T_1$, one can improve the fit of $M(t)$ with ILT and the resulting $P(1/T_1)$ would reveal two distinct peaks. The aforementioned kink observed around the delay time ~ 1 ms around 4.2 K is nicely reproduced in the ILT fit, and the resulting $P(1/T_1^{\rm Cu})$ has double peaks, as shown in Fig. **3a-b** in the main text. Typically, when the $M(t)$ data points have a random noise at the level of ~ 1 % or less, one can resolve two distinct values of $1/T_1$ in $P(1/T_1)$ separated by a half decade.

When the signal to noise ratio for the spin echo is extremely poor, it becomes difficult to conduct the ILT analysis. The scattering of $M(t)$ data points due to the random noise needs to be kept small; otherwise the Tikhonov regularization parameter α becomes larger (i.e. stronger smoothing) and $P(1/T_1)$ becomes broad, as discussed in section IV-B below. Under such circumstance, since the stretched fit analysis of $M(t)$ is generally more forgiving than ILT and does not require extremely good signal to noise ratio, $1/T_{1,\rm str}$ is still useful. Note that $1/T_{1,\rm str}$ is often very close to the center of gravity value $1/T_{1,\rm cg}$ of the distributed $1/T_1$, as shown in Fig. 2. This means that, without conducting ILT for $M(t)$ data measured with extremely high accuracy, one can substitute $1/T_{1,\rm str}$ as a crude estimation of $1/T_{1,\rm cg}$. For this reason, we did not attempt to deduce $P(1/T_1^{\rm Cu,Br})$ for $ZnCu_3(OD)_6FBr$ above ~ 60 K due to the very poor signal to noise ratio.

In Fig. S2(a), we compare the stretched fit $1/T_{1,\rm str}^{\rm Cu,Br,F}$ for $ZnCu_3(OD)_6FBr$ and $ZnCu_3(OD)_6Cl_2$ ("Hbt") in one panel to underscore the qualitative similarity in their temperature dependence below ~ 50 K. The corresponding stretched exponent β is summarized in Fig. S2(b) using the same symbols as in Fig. S2(a). In Fig. S3, we also summarize $1/T_{1,\rm str}^{\rm Cu}$ measured for $ZnCu_3(OD)_6FBr$ with $\tau = 6$, 15, and 30 μs. Notice that the $1/T_{1,\rm str}^{\rm Cu}$ results measured with a long delay time $\tau = 30$ μs is very similar to the singlet component $1/T_{1,\rm singlet}^{\rm Cu}$ in Fig. 2(a), deduced from the ILT analysis of the short delay time $\tau = 6$ μs. This is because the contribution by the ^{63}Cu nuclear spins with faster $1/T_{1,\rm para}^{\rm Cu}$ is suppressed for the longer delay time.

In Fig. S3, we overlaid the activation fit of $1/T_{1,\rm singlet}^{\rm Cu} = A_{\rm floor} + B \cdot exp(-\Delta/T)$ with a gap $\Delta = 28 \pm 5$ K. The

* Corresponding author: imai@mcmaster.ca

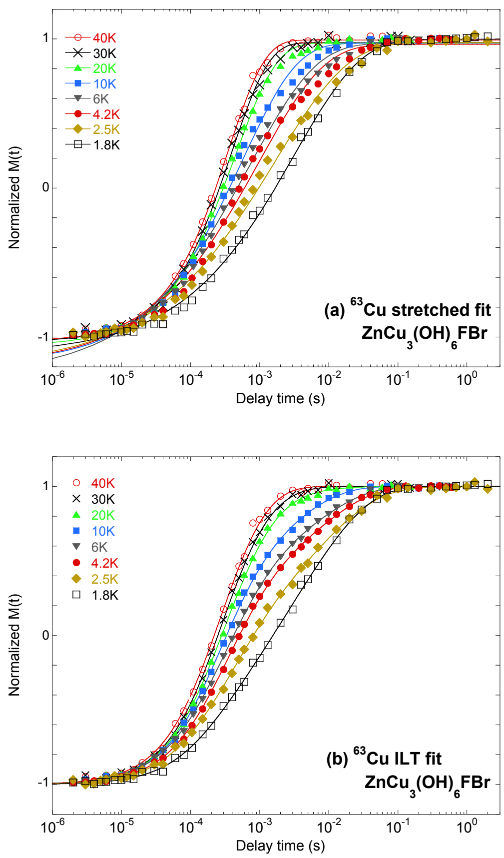

FIG. S1. (a) Examples of the stretched exponential fit of $M(t)$ observed at ^{63}Cu sites in $ZnCu_3(OD)_6FBr$. The fit becomes progressively poorer below 30 K, where a distinct slow mode emerges with increasing weight. (b) The same $M(t)$ curves fitted with the ILT. The fit is always good.

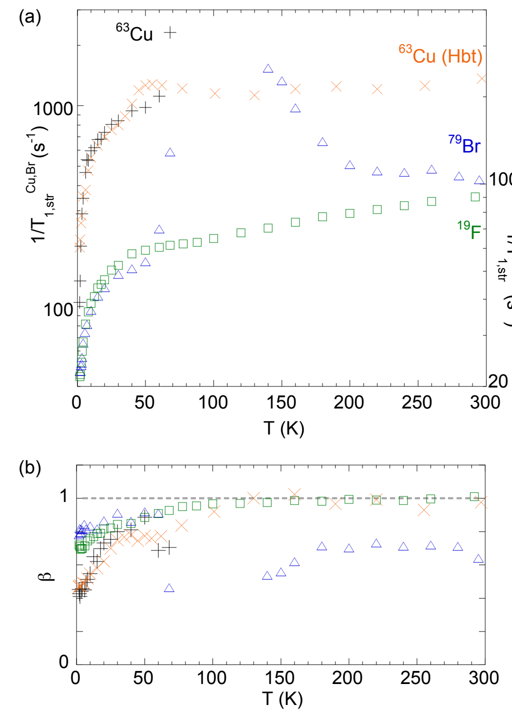

FIG. S2. (a) Temperature dependence of $1/T_{1,\mathrm{str}}^{\mathrm{Cu}}$ (+), $1/T_{1,\mathrm{str}}^{\mathrm{Br}}$ (blue △), and $1/T_{1,\mathrm{str}}^{\mathrm{F}}$ (green □) in $ZnCu_3(OD)_6FBr$ as determined by the conventional stretched fit of $M(t)$. Also shown is $1/T_{1,\mathrm{str}}^{\mathrm{Cu}}$ for $ZnCu_3(OD)_6Cl_2$ (orange ×). Notice that the temperature dependence of stretched fit $1/T_{1,\mathrm{str}}$ is similar at all sites below $\sim$ 50 K. This is simply because $1/T_{1,\mathrm{str}}$ is a crude approximation of the center of gravity value $1/T_{1,\mathrm{cg}}$ of the distributed $1/T_1$. (b) The corresponding stretched fit parameter β, shown using the same symbols as in panel (a).

estimated value of Δ is reasonable, in the sense that the singlet component in $P(1/T_1)$ becomes visible (and the fraction of spin singlets f_s becomes non-zero) below $\sim$ 30 K. But this large Δ should be considered the upper bound of the spatially distributed excitation gap for the singlets, because the activation fit of $1/T_{1,\mathrm{singlet}}^{\mathrm{Cu}}$ ignores the fact that the population f_s itself is temperature dependent. In fact, the increase of f_s below $\sim$ 10 K in Fig. 4 implies that the gap is comparable to 10 K or less for a significant fraction of singlets, but $1/T_{1,\mathrm{singlet}}^{\mathrm{Cu}}$ levels off at the floor value $A_{\mathrm{floor}} \gtrsim 20$ s^{-1} below 10 K due to the background contributions arising from defect spins. Accordingly, it is not trivial to deduce the distributed Δ from the temperature dependence of $1/T_{1,\mathrm{singlet}}^{\mathrm{Cu}}$.

The ^{63}Cu and ^{79}Br NQR intensity plotted in the inset of Fig. S3 decreases by up to a factor of $\sim$ 2 below $\sim$ 6 K in both $ZnCu_3(OD)_6FBr$ and $ZnCu_3(OD)_6Cl_2$. Our finding is consistent with the onset below $\sim$ 6 K of the slow spin dynamics observed by μSR experiments in these materials [2]. The lower error bars attached to f_s in Fig. 4 below 6 K marks the lower bound of f_s estimated based on the extreme assumption that the ^{63}Cu NQR signal intensity loss affects only the faster paramagnetic peak with $1/T_{1,\mathrm{para}}^{\mathrm{Cu}} \sim 1000$ s^{-1}. We emphasize that the lower bound of f_s still increases below $\sim$ 10 K.

II. EFG CONTRIBUTIONS TO $1/T_1$

In general, $1/T_1$ is proportional to the square of the nuclear gyromagnetic ratio γ_n^2, if the spin-lattice relaxation process is entirely dominated by magnetic effects. On the other hand, $1/T_1$ is proportional to the square of the nuclear quadrupole moment Q^2, if the nuclear quadrupole interaction dominates $1/T_1$ through the fluctuations of the electric field gradient (EFG).

In Fig. S4(a), we compare $1/T_{1,\mathrm{str}}^{\mathrm{Br}}$ measured for ^{79}Br isotope with the results for ^{81}Br divided by $(^{81}\gamma_n/^{79}\gamma_n)^2 = 1.16$. The good agreement between the two results below 50 K indicates that $1/T_{1,\mathrm{str}}^{\mathrm{Br}}$ is dominated by fluctuating hyperfine magnetic fields from Cu spins at low temperatures. On the other hand, the deviation of the results above $\sim$ 60 K shows that the

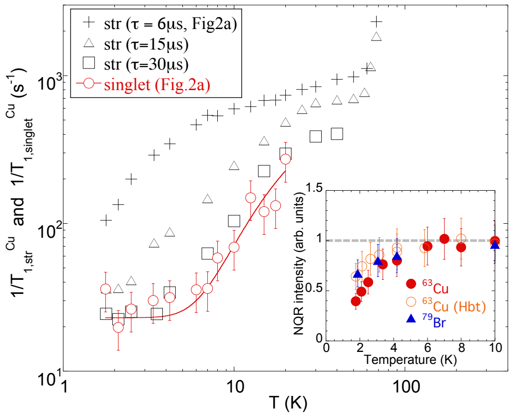

FIG. S3. Temperature dependence of the stretched fit $1/T_{1,\mathrm{str}}^{\mathrm{Cu}}$ measured with $\tau = 6$ μs (+, same data as in Fig. 2**a** and Fig. S2(a)), 15 μs ($\triangle$), and 30 μs ($\square$) in $\mathrm{ZnCu_3(OD)_6FBr}$. Also plotted is $1/T_{1,\mathrm{singlet}}^{\mathrm{Cu}}$ determined by the double Gaussian fit of $P(1/T_1^{\mathrm{Cu}})$ (red $\circ$, same data as in Fig. 2**a**). The solid curve through the data points of $1/T_{1,\mathrm{singlet}}^{\mathrm{Cu}}$ represents the activation fit with a gap $\Delta = 28 \pm 5$ K. Note that this Δ should be considered the upper-bound of the spatially distributed Δ. This is because the fit is treating all the $1/T_{1,\mathrm{singlet}}^{\mathrm{Cu}}$ data points on equal footing, despite the fact that the number of ^{63}Cu nuclear spins in the singlets gradually diminishes toward $\sim$ 30 K. Inset: The ^{63}Cu and ^{79}Br NQR intensity of $\mathrm{ZnCu_3(OD)_6FBr}$ (filled symbols) and $\mathrm{ZnCu_3(OD)_6Cl_2}$ ($\circ$), corrected for the Boltzmann factor by multiplying temperature. We used $\tau = 6$ μs for ^{63}Cu and $\tau = 15$ μs for ^{79}Br.

steep upturn of $1/T_{1,\mathrm{str}}^{\mathrm{Br}}$ is induced by fluctuating EFG instead, because the quadrupole moment is smaller for ^{81}Br, $(^{81}Q/^{79}Q)^2 = 0.70$. This finding is consistent with the fact that $1/T_{1,\mathrm{str}}^{\mathrm{F}}$ shows no corresponding enhancement above 60 K, because ^{19}F has nuclear spin $I = 1/2$, and hence nuclear quadrupole interaction has no contribution to $1/T_{1,\mathrm{str}}^{\mathrm{F}}$.

Superposition of the ^{79}Br NQR signals on ^{65}Cu NQR peak, shown in Fig. 1**d**, prevented us from confirming that the enhancement of $1/T_{1,\mathrm{str}}^{\mathrm{Cu}}$ observed above 60 K in $\mathrm{ZnCu_3(OD)_6FBr}$ is also caused by fluctuating EFG. However, ^{63}Cu and ^{65}Cu NQR peaks are isolated in $\mathrm{ZnCu_3(OD)_6Cl_2}$, and hence we were able to compare $1/T_{1,\mathrm{str}}^{\mathrm{Cu}}$ between ^{63}Cu and ^{65}Cu as shown in Fig. S4(b), where the ^{65}Cu results are normalized by $(^{65}\gamma_n/^{63}\gamma_n)^2 = 1.15$. In the inset of Fig. S4(b), we plot the ratio of $1/T_{1,\mathrm{str}}^{\mathrm{Cu}}$ between two isotopes. The ratio agrees with 1.15 except around 50 K, where $1/T_{1,\mathrm{str}}^{\mathrm{Cu}}$ exhibits a small hump. We can therefore conclude that this hump is also caused by EFG fluctuations. Again, this is consistent with the fact that $1/T_{1,\mathrm{str}}^{\mathrm{H}}$ measured at the ^{1}H sites of $\mathrm{ZnCu_3(OH)_6Cl_2}$ shows no hump [3], because ^{1}H has nuclear spin $I = 1/2$ and hence is immune from EFG, whereas $1/T_{1,\mathrm{str}}^{\mathrm{Cl}}$ measured at the quadrupolar ^{35}Cl sites ($I = 3/2$) also has a hump.

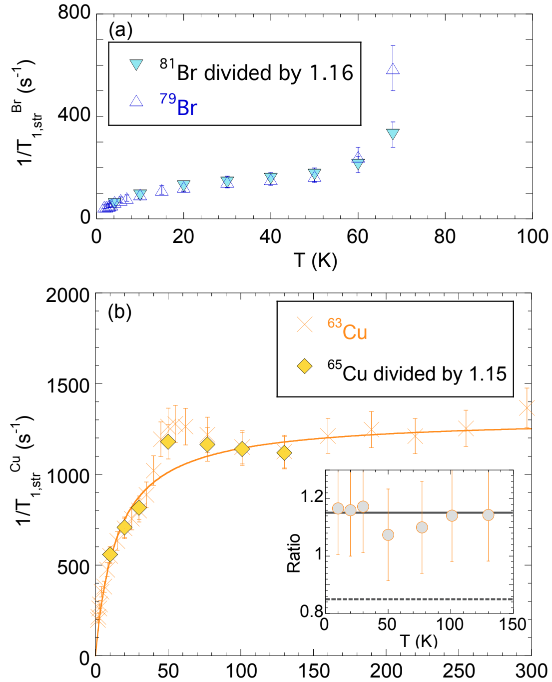

FIG. S4. (a) Comparison of $1/T_{1,\mathrm{str}}^{\mathrm{Br}}$ measured at ^{79}Br and ^{81}Br sites in $\mathrm{ZnCu_3(OD)_6FBr}$. The latter is normalized by dividing with $(^{81}\gamma_n/^{79}\gamma_n)^2 = 1.16$, the ratio expected if the relaxation is caused entirely by Cu spin fluctuations. (b) $1/T_{1,\mathrm{str}}^{\mathrm{Cu}}$ measured at ^{63}Cu and ^{65}Cu sites of $\mathrm{ZnCu_3(OD)_6Cl_2}$. The latter is normalized by dividing with $(^{65}\gamma_n/^{63}\gamma_n)^2 = 1.15$, the ratio expected if the relaxation is caused entirely by Cu spin fluctuations. Solid line represents the best fit assuming Curie-Weiss law for the dynamical spin susceptibility, $1/T_{1,\mathrm{str}}^{\mathrm{Cu}}T \propto (T+\theta)^{-1}$ with $\theta = 31$ K. Inset: the isotope ratio of $1/T_{1,\mathrm{str}}^{\mathrm{Cu}}$ between ^{65}Cu and ^{63}Cu isotopes. We expect the ratio to be 1.15 for entirely magnetic process (horizontal solid line), and 0.85 for entirely quadrupole process (horizontal dotted line). The dip around 50 K implies that EFG fluctuations make additional contributions to $1/T_{1,\mathrm{str}}^{\mathrm{Cu}}$, and enhances the overall relaxation rate.

III. CONSISTENCY CHECKS OF THE TWO COMPONENT NATURE OF $P(1/T_1^{\mathrm{Cu}})$

A. Two-component fit of $M(t)$ in the time domain

The presence of two peaks in $P(1/T_1^{\mathrm{Cu}})$ in Fig. 3**a** indicates that there are two distinct environments for ^{63}Cu nuclear spins in $\mathrm{ZnCu_3(OD)_6FBr}$ below $\sim$ 30 K with up to two orders of magnitude different values of $1/T_1^{\mathrm{Cu}}$. This, in turn, implies that the recovery curve $M(t)$ itself has two distinct contributions with fast and slow relaxation rates, $1/T_{1,\mathrm{fast}}^{\mathrm{Cu}}$ and $1/T_{1,\mathrm{slow}}^{\mathrm{Cu}}$, corresponding to $1/T_{1,\mathrm{para}}^{\mathrm{Cu}}$ and $1/T_{1,\mathrm{singlet}}^{\mathrm{Cu}}$, respectively. In fact, eye inspection of $M(t)$ observed at 4.2 K (reproduced from Fig. 1**g** in Fig. S5(a)) initially recovers as quickly as at

40 K until the delay time reaches $t \sim 10^{-3}$ s, after which a slow recovery mode takes over.

One can verify the existence of two distinct modes in $M(t)$ in the time domain with the two-component stretched fit of $M(t)$: $M(t) = M_o - A \cdot exp[-(3t/T_{1,\mathrm{fast}}^{\mathrm{Cu}})^{\beta}] - A' \cdot exp[-(3t/T_{1,\mathrm{slow}}^{\mathrm{Cu}})^{\beta'})]$. This fitting function, however, has as many as 7 free parameters, M_o, A, $1/T_{1,\mathrm{fast}}^{\mathrm{Cu}}$, β, A', $1/T_{1,\mathrm{slow}}^{\mathrm{Cu}}$, and β', and hence the stability of the fit proved to be inadequate. We therefore introduced a constraint, $\beta = \beta'$, to stabilize the fit. This makes sense and is justifiable, because the widths of the two peaks in $P(1/T_1^{\mathrm{Cu}})$ are comparable in Fig. 3**a**, and hence the fast and slow modes should have comparable distributions in $1/T_{1,\mathrm{fast}}^{\mathrm{Cu}}$ and $1/T_{1,\mathrm{slow}}^{\mathrm{Cu}}$.

Notice that the two-component stretched fit in Fig. S5(a) (red solid curve) works much better than the single component stretched fit (black dashed curve in Fig. 1**g**, or equivalently the solid red curve in Fig.S1(a)), and properly reproduces the kink located at the delay time $t \sim 10^{-3}$ s. The $\chi^2 = 8.65 \times 10^{-4}$ for the two-component stretched fit is reduced by a factor of 33 from $\chi^2 = 2.85 \times 10^{-2}$ for the single-component stretched fit.

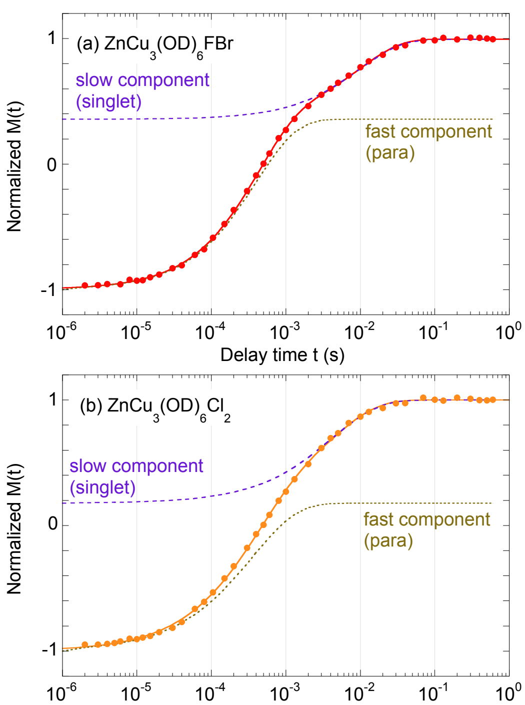

FIG. S5. (a) Red bullets: $M(t)$ of ^{63}Cu sites in $ZnCu_3(OD)_6FBr$ observed at 4.2 K (reproduced from Fig. 1**g**). Solid red curve shows the best two-component stretched fit as described in section III-A. Brown dotted curve and purple dashed curve represent the deconvolution into the fast and slow components with $1/T_{1,\mathrm{fast}}^{\mathrm{Cu}} = 830$ s^{-1} and $1/T_{1,\mathrm{slow}}^{\mathrm{Cu}} = 33$ s^{-1}, respectively. (b) Analogous deconvolution of $M(t)$ for ^{63}Cu sites in $ZnCu_3(OD)_6Cl_2$.

Moreover, $1/T_{1,\mathrm{fast}}^{\mathrm{Cu}} = 830$ s^{-1} and $1/T_{1,\mathrm{slow}}^{\mathrm{Cu}} = 33$ s^{-1} are in excellent agreement with the estimation based on the double Gaussian deconvolution of $P(1/T_1^{\mathrm{Cu}})$ in Fig. 3a, $1/T_{1,\mathrm{para}}^{\mathrm{Cu}} = 831$ s^{-1} and $1/T_{1,\mathrm{singlet}}^{\mathrm{Cu}} = 32$ s^{-1}, respectively. In addition, the fraction of the slow component $A'/(A + A') = 0.32$ agrees well with $f_s = 0.30$ estimated from the deconvolution of the ILT results of $P(1/T_1^{\mathrm{Cu}})$. Therefore, the two-component analysis of $M(t)$ in the time domain is indeed consistent with the two-component nature of $P(1/T_1^{\mathrm{Cu}})$ found in the ILT analysis.

Plotted in Fig. S5(b) are the corresponding deconvolution of $M(t)$ for $ZnCu_3(OD)_6Cl_2$ at 4.2 K. We obtain $1/T_{1,\mathrm{fast}}^{\mathrm{Cu}} = 950$ s^{-1}, $1/T_{1,\mathrm{slow}}^{\mathrm{Cu}} = 78$ s^{-1}, and $A'/(A + A') = 0.41$. These fit parameters are again in very good agreement with the ILT results in Fig. 3**b** and Fig. 4, although the two component fit appears hardly justifiable unless one knows the ILT results of $P(1/T_1)^{\mathrm{Cu}}$ in Fig. 3**b**. Moreover, without introducing the constraint $\beta = \beta'$, the two component fit is not stable. A major advantage of the ILTT$_1$ analysis is that one needs not make any assumption for the functional form of $M(t)$ up front. If $M(t)$ encompasses two distinct modes, $P(1/T_1^{\mathrm{Cu}})$ would show two peaks, as long as the separation between two peaks is greater than the effective resolution of ILT.

B. $1/T_{1,\mathrm{str}}^{\mathrm{Cu}}$ measured with $\tau = 30$ μs

As an additional check, we also measured $1/T_{1,\mathrm{str}}^{\mathrm{Cu}}$ with a longer pulse separation time $\tau = 30$ μs between the 90 and 180 degree pulses, and compared the results with $1/T_{1,\mathrm{singlet}}^{\mathrm{Cu}}$ in Fig. S3. They show nearly identical behavior. This implies that the recovery curve measured with $\tau = 30$ μs no longer has the faster paramagnetic component $1/T_{1,\mathrm{para}}^{\mathrm{Cu}}$. In fact, as shown in Fig. S9 below, the paramagnetic peak of $P(1/T_1^{\mathrm{Cu}})$ centered around $1/T_{1,\mathrm{para}}^{\mathrm{Cu}} \simeq 1000$ s^{-1} is progressively suppressed for longer values of τ due to faster transverse relaxation, and only the singlet peak centered around $1/T_{1,\mathrm{singlet}}^{\mathrm{Cu}}$ remains for $\tau = 30$ μs. These findings provide additional evidence that two distinct environments exist for ^{63}Cu sites at low temperatures.

IV. ILTT$_1$ ANALYSIS

A. The principles of ILT

The procedures of the ILTT$_1$ analysis were initially developed and applied in petrophysics over the last two decades [4–6]. We refer readers to section II of ref.[1] for a brief overview of what one can do with ILT, and the Supplemental Materials of ref.[1, 7] for the detailed procedures of the ILT fits, including how to optimize the Tikhonov regularization parameter α, and how to treat incomplete inversion of $M(t)$ at short delay time. In what follows, we summarize the key aspects of ILT briefly.

In the ILTT$_1$ analysis, we find the probability density $P(1/T_{1\mathrm{j}})$ for the j-th value of $1/T_1$ by inverting the recovery curve $M(t) = \sum_j P(1/T_{1\mathrm{j}})\ \{1 - 2\ exp(-ct/T_{1\mathrm{j}})\}$. Note that, technically, this is the discrete form of a Fredholm integral equation of the first kind, but for simplicity we refer to it here as an ILT. To achieve our goal, we use the Tikhonov regularization method to find the solution $\mathbf{P}$ [1] :

$$\mathbf{P} = \underset{\mathbf{P}\geq 0}{\arg\min}\ ||\mathbf{M} - K\,\mathbf{P}||^2 + \alpha||\mathbf{P}||^2, \tag{1}$$

where $||..||$ is the vector norm, and

$$\begin{aligned} \mathbf{M} &= \{M(t_i), i = 1, ..., n\}\,, \\ K &= \left\{K_{ij} = \left[1 - 2e^{-ct_i/T_{1\mathrm{j}}}\right]\right\}, \\ \mathbf{P} &= \{P(1/T_{1\mathrm{j}}), j = 1, ..., m\}\,. \end{aligned} \tag{2}$$

K is the kernel matrix of size $n \times m$. The pre-factor $c = 3$ for the nuclear spin $I_z = \pm 3/2$ to $\pm 1/2$ transitions of ^{63}Cu and ^{79}Br NQR, and $c = 1$ for the nuclear spin $I_z = +1/2$ to $-1/2$ transition of ^{19}F NMR. The number of measured data points is typically $n \simeq 40$, and $m = 250$ is the chosen number of logarithmically spaced bins in the $P(1/T_1)$ distribution. α is the scalar regularization parameter (i.e. a smoothing factor) chosen to be large enough to make the solution stable in the presence of noise. In essence, α determines the degree of smoothing for $P(1/T_1)$, and becomes larger if $M(t)$ has greater random noise. If α is too large, the resultant $P(1/T_1)$ becomes too broad. On the other hand, if α is too small due to improper optimization, the resultant probability density $P(1/T_1)$ becomes "spiky" and will have artificial peaks.

We normalize the total integral of $P(1/T_1)$ in the log scale to 1 so that the integral of $P(1/T_1)$ between $1/T_1 = a$ to $1/T_1 = b$ gives the probability of $1/T_1$ in the range between a and b. If $1/T_1$ is distributed around the single value of d, the ILT of $M(t)$ will result in $P(1/T_1)$ peaked at $1/T_1 = d$. On the other hand, if $1/T_1$ is distributed around two distinct values d and g, $P(1/T_1)$ would have two corresponding peaks at d and g, as was the case for ^{63}Cu in Fig. 3**a**; see Fig. 1 of ref.[1] for a concrete example based on a forward model consisting of two different values of $1/T_1$. Typically, one can resolve two peaks of $P(1/T_1)$ if the separation between them is a half decade or greater.

B. General consideration on the relation between α and the width of $P(1/T_1)$

In this subsection, we will illustrate the extra width introduced to $P(1/T_1)$ by the ILT process itself in order to provide the general sense on the effective "resolution" of $P(1/T_1)$. In what follows, we consider a model system with $1/T_1 = 1000\ \mathrm{s}^{-1}$ with no distribution. We generate $M(t)$ with 1% built-in random noise, then calculate $P(1/T_1)$ for various values of fixed α as shown in Fig. S6(a). Note that $P(1/T_1)$ becomes broader for larger values of α, even though the original $M(t)$ has no distribution in $1/T_1$.

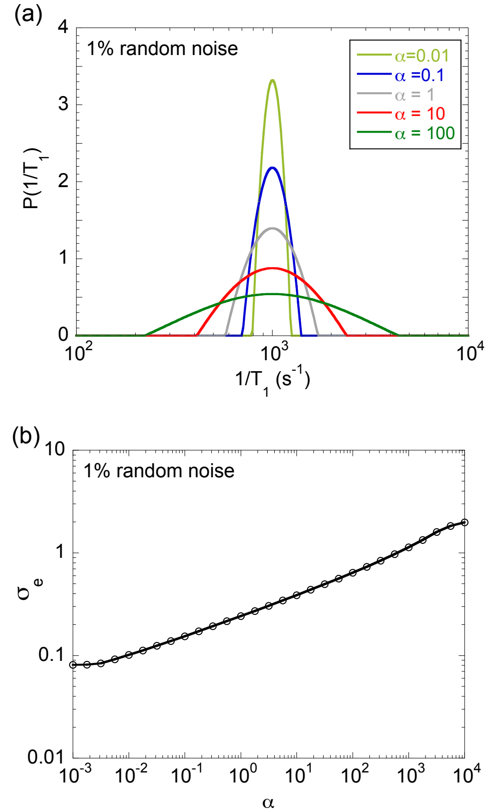

FIG. S6. (a) $P(1/T_1)$ calculated with various α for a model recovery curve $M(t)$ with $1/T_1 = 1000\ \mathrm{s}^{-1}$ without any distribution, but with 1% built-in random noise (or, signal-to-noise ratio SNR = 100, equivalently). In an ideal situation, $P(1/T_1)$ calculated from such $M(t)$ should become a delta function, but the finite value of α introduces an apparent distribution in $P(1/T_1)$. (b) The standard deviation σ_e on a natural log scale calculated for the $P(1/T_1)$ curves.

We then calculate the standard deviation σ_e on a natural logarithmic scale for these $P(1/T_1)$ curves (i.e. the width), and summarize its α dependence in Fig. S6(b). If we approximate $P(1/T_1)$ as a Gaussian function on a log scale, we can estimate $1/T_1$ at the upper (or lower) half height as $1000 \times exp(+2ln(2)\sigma_e)$ (or $1000 \times exp(-2ln(2)\sigma_e)$), where the pre-factor 1000 is the central value of $1/T_1$ assumed in the model. Generally, we keep averaging the spin echo signal to reduce the noise, until the random scattering of the $M(t)$ data becomes $\sim 1\%$ or less. In the case of our ^{63}Cu NQR measurements, the standard optimization procedures led to $\alpha \simeq 3$ as shown in the next section, from which we find $\sigma_e \simeq 0.3$ using Fig. S6(b). This means that the paramagnetic peak of $P(1/T_1^{\mathrm{Cu}})$ centered at $1/T_{1,\mathrm{para}} = 1000\ \mathrm{s}^{-1}$ is subjected to the extra width in the range between $1/T_1 \simeq 1400$ and $700\ \mathrm{s}^{-1}$ by the ILT itself, as shown by the thick horizontal

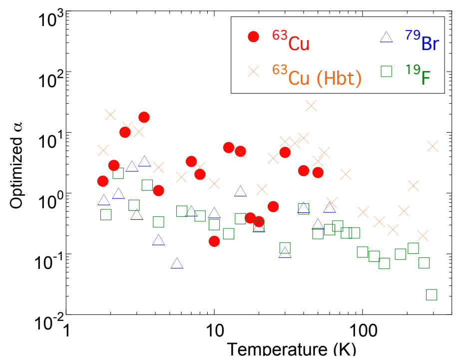

FIG. S7. Temperature dependence of the optimized values of α for $ZnCu_3(OD)_6FBr$ and for the ^{63}Cu sites of $ZnCu_3(OD)_6Cl_2$ ($\times$).

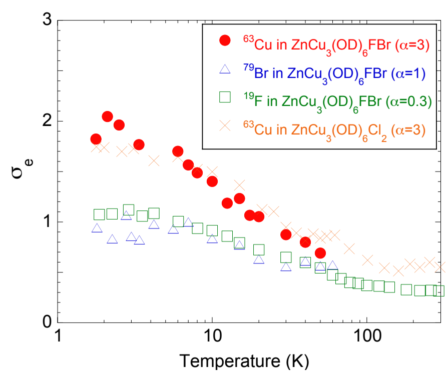

FIG. S8. The standard deviation σ_e on a log scale (i.e. the width) calculated for $P(1/T_1)$.

bar in the upper right corner of Fig. 3(a).

The key message here is that $P(1/T_1)$ ends up with a finite width, even if there is no distribution in $1/T_1$, because the experimental data of $M(t)$ always has some random noise and the ILT smooths it out with a finite α. The half width at the half maximum set by σ_e gives us a crude estimation of the upper bound of the effective *resolution* of our ILTT$_1$ analysis, or equivalently, the minimum extra width. (Our estimation should be considered the minimum extra width, because $P(1/T_1)$ with more complicated shape could have larger width for the same value of α).

C. Temperature dependence of ILT parameters

We summarize the optimized value of α in Fig. S7. To avoid the randomness in the extra width introduced by the ILT itself, we take the average value $\alpha = 3$, 1, and 0.3 for ^{63}Cu, ^{79}Br and ^{19}F, respectively, and re-calculated $P(1/T_1)$ for Figs. 2 and 3 using these fixed values of α.

In Fig. S8, we summarize the temperature dependence of σ_e on a log scale calculated for $P(1/T_1)$. σ_e shows qualitatively similar broadening at all sites at lower temperatures. The increased inhomogeneity in the magnetic properties of the kagome planes does not lead to the emergence of the split-off peak of $P(1/T_1)$ at ^{79}Br and ^{19}F sites, simply because these sites probe the average behavior of the 6 or 12 neighboring Cu^{2+} sites, respectively. It is also worth recalling that the temperature dependence of σ_e generally anti-correlates with that of β shown in Fig. S2(b) [1]. When the distribution of $1/T_1$ grows, σ_e grows and the stretched exponent deviates more strongly from $\beta = 1$.

D. τ dependence of $P(1/T_1^{\mathbf{Cu}})$

In Fig. S3 above, we showed that the behavior of $1/T^{\mathrm{Cu}}_{1,\mathrm{singlet}}$ can be singled out by measuring $1/T_1$ with a longer $\tau = 30$ μs. To further illustrate the presence of the split-off peak in $P(1/T_1^{\mathrm{Cu}})$, we compare the $P(1/T_1^{\mathrm{Cu}})$ observed at 4.2 K for various values of τ in Fig. S9. Notice that the paramagnetic peak centered at $1/T^{\mathrm{Cu}}_{1,\mathrm{para}} \simeq 1000$ s^{-1} is progressively suppressed for longer values of τ due to the faster transverse relaxation, and only the singlet peak centered at $1/T^{\mathrm{Cu}}_{1,\mathrm{singlet}}$ remains at $\tau = 30$ μs.

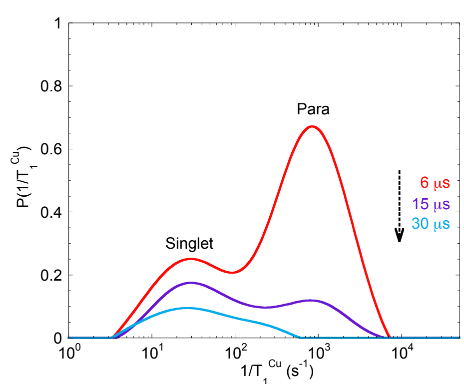

FIG. S9. $P(1/T_1^{\mathrm{Cu}})$ of $ZnCu_3(OD)_6FBr$ measured with various values of the 90°-180° pulse separation time τ at 4.2 K. Note that only the singlet peak remains at $\tau = 30$ μs. The result for $\tau = 6$ μs is the same as in Fig. 3**a**, and the integrated area is normalized to 1. For longer τ values, the integrated area is scaled with the overall spin echo intensity estimated from the M_o value in each $1/T_1$ measurement.

[1] Singer, P. M., Arsenault, A., Imai, T. & Fujita, M. ^{139}La NMR investigation of the interplay between lattice, charge, and spin dynamics in the charge-ordered high-T_c cuprate $La_{1.875}Ba_{0.125}CuO_4$. *Phys. Rev. B* **101**, 174508 (2020).

[2] Tustain, K. *et al.* From magnetic order to quantum disorder: a μSR study of the Zn-barlowite series of S=1/2 kagomé antiferromagnets, $Zn_xCu_{4-x}(OH)_6FBr$. *Nature Comm.* **5**, 74 (2020).

[3] Imai, T., Nytko, E. A., Bartlett, B. M., Shores, M. P. & Nocera, D. G. ^{63}Cu, ^{35}Cl, and ^{1}H NMR in the $S = \frac{1}{2}$ Kagome Lattice $ZnCu_3(OH)_6Cl_2$. *Phys. Rev. Lett.* **100**, 077203 (2008).

[4] Song, Y. Q. *et al.* T_1-T_2 correlation spectra obtained using a fast two-dimensional Laplace inversion. *J. of Magn. Res.* **154**, 261–268 (2002).

[5] Venkataramanan, L., Song, Y. Q. & Hurlimann, M. D. Solving Fredholm Integrals of the First Kind with Tensor Product Structure in 2 and 2.5 Dimensions. *IEEE Trans. Sig. Process.* **50**, 1017 (2002).

[6] Singer, P. M., Asthagiri, D., Chapman, W. G. & Hirasaki, G. J. NMR spin-rotation relaxation and diffusion of methane. *J. Chem. Phys.* **148**, 164507 (2018).

[7] Arsenault, A., Imai, T., Singer, P. M., Suzuki, K. M. & Fujita, M. Magnetic inhomogeneity in charge-ordered $La_{1.885}Sr_{0.115}CuO_4$ studied by NMR. *Phys. Rev. B* **101**, 184505 (2020).